Versatile Polymer-Free Graphene Transfer Method and Applications

Guohui Zhang, † Aleix G. Güell, † * Paul M. Kirkman, Robert A. Lazenby, Thomas S. Miller and Patrick R. Unwin*

Department of Chemistry, University of Warwick, Coventry, CV4 7AL, United Kingdom.

Corresponding Author

* To whom correspondence should be addressed. E-mail: p.r.unwin@warwick.ac.uk; a.g.guell@warwick.ac.uk.

† These authors contributed equally.

Keywords: graphene transfer, free-standing graphene, conductive AFM, graphene TEM grids, electrochemistry.

Abstract

A new method for transferring chemical vapor deposition (CVD)-grown monolayer graphene, to a variety of substrates is described. The method makes use of an organic/aqueous biphasic configuration, avoiding the use of any polymeric materials that can cause severe contamination problems. The graphene-coated copper foil sample (on which graphene was grown) sits at the interface between hexane and an aqueous etching solution of ammonium persulfate to remove the copper. With the aid of an Si/SiO_2 substrate, the graphene layer is then transferred to a second hexane/water interface, to remove etching products. From this new location, CVD graphene is readily transferred to arbitrary substrates, including three dimensional architectures as represented by atomic force microscopy (AFM) tips and transmission electron microscopy (TEM) grids. Graphene produces a conformal layer on AFM tips, to the very end, allowing the easy production of tips for conductive AFM imaging. Graphene transferred to copper TEM grids provides large area, highly electron-transparent substrates for TEM imaging. These substrates can also be used as working electrodes for electrochemistry and high resolution wetting studies. By using scanning electrochemical cell microscopy, it is possible to make electrochemical and wetting measurements at either a free-standing graphene film or a copper-supported graphene area, and readily determine any differences in behavior.

Introduction

Since its discovery in 2004,[1] the outstanding electrical,[2, 3] mechanical[4, 5] and chemical[6, 7] properties of graphene have been revealed, highlighting it as a hugely promising material for the future. The production of pristine graphene flakes was initially achieved through a (Scotch-tape based) mechanical exfoliation[1] method. However, with this time-consuming approach typically yielding micron-sized flakes, it is considered unrealistic for scale up applications, where much larger areas of graphene are needed.[8, 9]

Recently, chemical vapor deposition (CVD) has shown considerable promise for the synthesis of large-scale (with sheets of 30 inches in size reported[10]), high-quality graphene.[11-13] Among the metals used to catalyze the CVD growth of graphene, copper (Cu) is the most popular, producing mostly monolayer graphene.[14] However, depending on the application, an effective methodology for the subsequent transfer of such films to substrates of interest is still required.[15] This is far from easy, especially when a large, continuous sheet is desired, or three-dimensional (3D) structures are to be covered. Polymer support routes have been extensively employed for such transfer, in which a thin layer of polymer is deposited as a new support (template) on the as-grown (metal-supported) graphene, to allow the removal of the metallic substrate by wet etching or electrochemical delamination, ultimately producing a polymer-supported graphene film.[16, 17] Polymethylmethacrylate (PMMA),[18] polydimethylsiloxane (PDMS)[19] and polycarbonate[20] layers (among others) are reported as suitable templates for the transfer of graphene onto a wide variety of planar/flat substrates, with the polymer subsequently removed through dissolution with organic solvents. Despite intensive research into such methods, the resulting graphene surfaces commonly appear littered with stubborn polymer residues,[21, 22] which may have a detrimental effect on subsequent applications, including the electronic and electrochemical performance of

graphene.[23, 24] Consequently, alternative routes of transfer are being sought, with polymer-free methods recently emerging as a fresh and promising way for clean graphene transfer.[25, 26]

Herein, we introduce a polymer-free biphasic (liquid/liquid) approach for the transfer of monolayer CVD graphene to a wide range of target substrates. Our approach makes use of an inert non-polar and low viscosity liquid organic layer (hexane) lying on top of an aqueous etchant layer (ammonium persulphate, $(NH_4)_2S_2O_8$), to stabilize and protect the free-standing graphene sheet that is produced during the Cu wet etching and water rinsing processes. Essentially, the hexane layer replaces the deposited polymer layers used in the majority of current graphene transfer methods (*vide supra*), ensuring the freestanding graphene produced after etching of the growth substrate is not torn apart by the surface tension associated with the aqueous etchant solution. Crucially, the lack of heteroatoms and aromatic groups in hexane, as well as its volatility and rapid evaporation, ensures that no residues are left on the graphene surface and that there is no doping after transfer to the desired substrate. Note that, although an organic/water interface was recently used to decorate CVD graphene films with nanoparticles, the process used still relied on polymer coating and removal.[27]

Additionally, we demonstrate the feasibility and versatility of our approach for coating graphene onto coarse surfaces and 3D structures, due to the gentleness of the polymer-free transfer method. Beyond flat substrates (e.g. Si/SiO_2), monolayer graphene membranes have been transferred to more topographically challenging substrates, such as atomic force microscopy (AFM) tips and transmission electron microscopy (TEM) grids. The resulting graphene-coated AFM tips and graphene TEM grids open up novel scientific avenues, for example, new capability for conductive AFM mapping and atomic-resolution TEM imaging of nanoparticles. Our method is also very suitable for the production of suspended graphene layers, an important goal in graphene science and technology to understand substrate effects on the resulting graphene properties.[28, 29] Indeed, facilitated by this transfer method, we

introduce the first studies on the wettability and electrochemistry of suspended graphene sheets.

Results and discussion

Polymer-free Transfer of CVD Graphene

The polymer-free biphasic transfer method is illustrated schematically in Figure 1. Monolayer graphene was grown on polycrystalline Cu foils in a low-pressure commercial CVD system, using methane as the carbon source (see Methods). After polishing the back of the Cu foil (to remove the graphene grown on the backside), the sample was initially floated (graphene side up) atop a 0.1 M $(NH_4)_2S_2O_8$ etching solution, which has been shown to minimize residues compared to the other commonly used $FeCl_3$ and $Fe(NO_3)_3$ solutions.[9, 30] At this point, a non-polar hexane layer was gently added dropwise to the surface of the etchant solution with a syringe, so that the graphene/Cu sample was trapped at the resulting organic/aqueous biphasic interface, with the exposed face of the hydrophobic graphene in contact only with the hexane, and the Cu foil exposed to the etchant solution. After sufficient etching time (~12 h), only the synthesized graphene sheet remained trapped at the interface. Note that the surface tension for the hexane/water interface is ca. 45 mN m^{-1}, [26, 31] lower than that of the air/water interface, which prevents the water layer pulling the sheet apart, as would be the case if the non-polar layer were not present.[26] The 'soft support' from the hexane layer also protects the graphene sheet by minimizing physical drift at the interface.

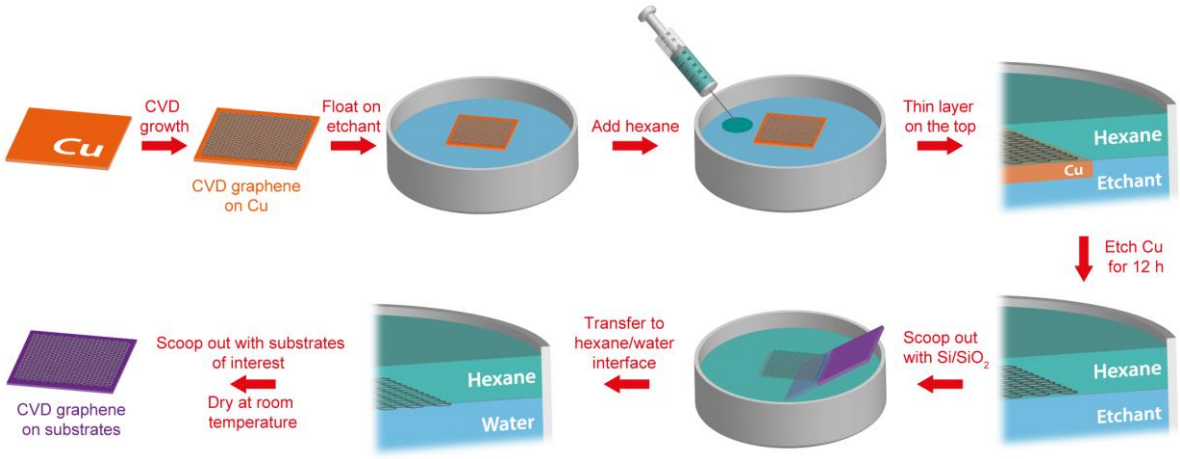

Figure 1 Schematic of the polymer-free biphasic method for CVD graphene transfer.

To further minimize any possible contamination from etchant salts produced, the monolayer graphene sheet was scooped out and transferred to a new hexane/pure water interface with the aid of an Si/SiO_2 wafer. After this cleaning step, the free-standing graphene sheet was scooped out from the interface using an arbitrary substrate of interest (e.g. Si/SiO_2 wafers, AFM tips and TEM grids for the studies herein) in a single swift motion, before being left to dry at room temperature (see Supporting Information (SI), section S1).

Salient observations from an etching process are presented in Figure 2. As shown in Figures 2a to 2c, there is a gradual etching of the copper foil, eventually leading to a complete and highly transparent graphene film of large area floating at the interface and maintaining its integrity. At this stage, the graphene film was ready to be transferred with a silicon wafer to a new hexane/pure water interface for 5 h, for the removal of any excess etchant salts (Figure 2d shows the start of this process). A video 'transfer.AVI' demonstrating the final transfer onto an Si/SiO_2 wafer can be downloaded as part of the SI.

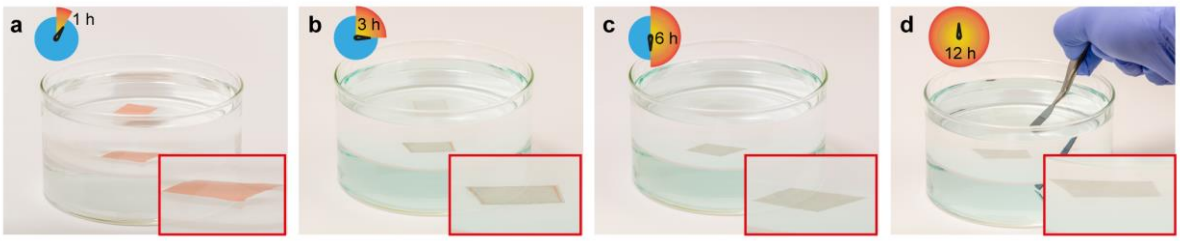

Figure 2 (a)-(c) Optical images of an as-grown graphene/copper sample floating at the interface between a hexane layer and a 0.1 M $(NH_4)_2S_2O_8$ aqueous solution during etching. (d) Optical image of the initial moments of the graphene film being scooped out by means of an Si/SiO_2 substrate. A video in the SI shows the rest of the transfer process.

A clean and complete graphene film was transferred onto Si/SiO_2, as evident by the optical and AFM images obtained after transfer (see SI, section S2). Raman spectroscopy measurements were also carried out to characterize the graphene samples (see SI, section S3). The Raman spectrum of graphene on copper showed a pronounced 2D band at 2664 cm^{-1} and a small G band at 1587 cm^{-1}, with almost no detectable D peak observed. This indicates the CVD growth of relatively high quality monolayer graphene.[19, 22, 32] When the graphene sheet was fully transferred onto an Si/SiO_2 wafer using our polymer-free transfer method, the intensity ratio of the 2D and G peaks (I_{2D}/I_G) was >2, with an associated full width at half-maximum (FWHM) for the 2D band of ~28 cm^{-1}, reaffirming the monolayer nature of the graphene grown. There was a small D band (at 1333 cm^{-1}) in the Raman spectrum of graphene on Si/SiO_2, with a D band intensity (I_D) to G band intensity (I_G) ratio of 0.11, being relatively uniform on the transferred graphene, as shown by the Raman map. This value suggests that relatively low-defect CVD graphene [33] was obtained by our growth and transfer process, of similar structural quality to that from polymer-assisted transfer methods commonly used in the literature (see SI, section S4).[28]

Fabrication and Utilization of Conductive Graphene AFM tips

Sheets of graphene find interesting use as an ultrathin template for the characterization of nanoscale structures trapped on a substrate, including molecules,[34] nanoparticles[35] and biological entities (e.g. bacteria[36] or viruses[37]). The polymer-free biphasic method is attractive for the coating of fragile, small and coarse substrates. We exemplified this capability by coating AFM probes with free-standing graphene films.

CVD graphene films were deposited onto AFM probes following the biphasic procedure described in the previous section (also see Methods). After the transfer, the presence of graphene on the AFM probe cantilever was observable under an optical microscope. The tips were further characterized with scanning electron microscopy (SEM) (Figures 3a and 3b) and TEM (Figure 3c), from which relatively few superficial features can be assigned to folds and wrinkles of the monolayer graphene. The images prove that the layer of graphene conforms very well to the AFM tip geometry, appearing to coat the AFM tip entirely, as well as the back of the cantilever by wrapping around it. Importantly, for AFM probe applications, we were interested in determining that the tip apex was also coated continuously with graphene, and to discard the possibility of a perforation of the graphene film by the very sharp end of the tip. TEM imaging (see Figure 3c) of graphene-coated AFM tips confirmed the presence of a continuous thin layer at the end of the tip, assigned to the graphene sheet. An attribute of the graphene coating is the thinness of the layer so that there is little change of the tip radius of curvature after coating to produce a conductive tip. This contrasts with metal-coated AFM tips, where several 10s of nm are typically deposited to make a conducting tip,[38, 39] with an impact on the spatial resolution of the imaging probe.

We converted as-prepared graphene-coated AFM tips into conductive AFM probes, by evaporating a continuous gold thin film onto the back of the AFM tip chip, wrapped by the graphene layer, to which an electrical contact was made (see the schematics in Figure 3d).

Simultaneous AFM maps of topography and electrical conductivity of highly oriented pyrolytic graphite (HOPG) were recorded. This substrate was chosen for the well-known structure and the electrical heterogeneity of its surface after exfoliation.[40, 41] As shown in Figure 3e, the surface presents several graphitic planes that show distinct electrical conductivity, in agreement with the behavior previously reported employing metal-coated AFM probes for its characterization.[40-43] We found that a single tip could be used for more than 50 hours for conductive AFM measurements without noticeable deterioration in performance (a total of > 50 images, each of a 5 μm × 5 μm area). Our transfer method brings to the fore a quick and easy approach for making these tips. Such conducting probes may also serve as a platform for molecular junctions,[44] and other applications, e.g. in electrochemistry and electrochemical imaging.

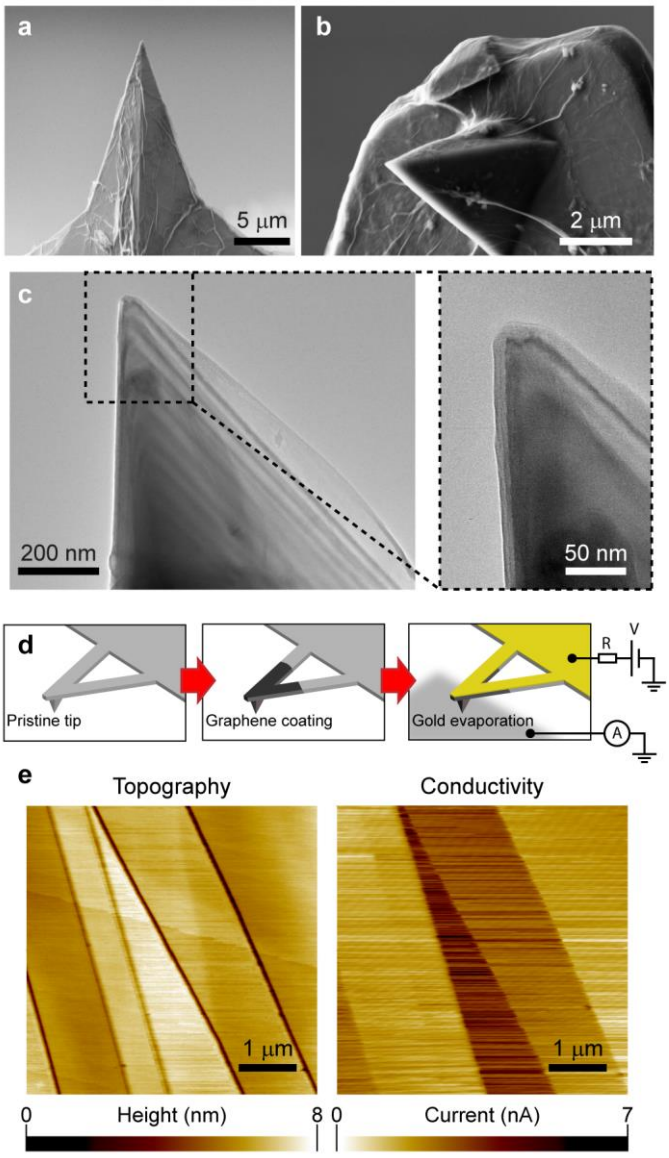

Figure 3 (a)-(b) SEM images of two graphene-coated AFM tips. (c) TEM images of the end of a graphene-coated AFM tip. (d) Schematic illustration of the production of a conductive AFM probe by coating graphene on a commercial tip, followed by gold evaporation on the back. (e) Topography and conductivity maps for a 5 μm × 5μm area of high quality highly oriented pyrolytic graphite (HOPG), utilizing a graphene-coated conductive AFM tip. Experimental details are given in Methods.

Graphene Coating on TEM Grids

There is currently considerable interest in using graphene films as supports for TEM measurements.[45-47] However, most processes to deposit graphene on holey TEM grids use polymer-assisted routes.[48] One study that was free of polymer, however, involved the etching of an Si/SiO_2 layer, but this is time-consuming and possibly introduces more contaminants to the graphene surface.[49]

In this study, we employed the biphasic graphene transfer method to produce TEM grids with one continuous single layer of CVD graphene as a support (see Methods). This represents a simple, cheap and quick route to obtain graphene TEM substrates. The original TEM grids were in the form of Cu meshes with holes (11.5 μm × 11.5 μm), so that the transfer of graphene resulted in sections with a suspended graphene membrane (across the holes) and a supported graphene film (on the Cu grid). After the transfer, the coverage was complete for the majority of the grid, and an area of the as-prepared graphene TEM grid was characterized by AFM and SEM (Figure 4). In the AFM image of Figure 4a, a partially-coated hole in the upper left corner is deliberately displayed to present the contrast between covered-uncovered regions. The whole layer of graphene is therefore well-coated across the grid, with regions of suspended graphene membrane slightly subsiding from the surrounding Cu bars, but remaining continuous, due to its strong mechanical properties (SI, section S5).

SEM images of a partially-covered hole, at the edge of graphene film (Figure 4b-d), show that the graphene film provides an excellent conformal coating over the relatively coarse Cu surface, as was also found for AFM tips. An important factor responsible for the excellent coating is the evaporation of water and hexane trapped between the graphene sheet and the TEM grid after the transfer which can act to pull both materials into intimate contact.[25, 49] Compared with transfer methods that are assisted by relatively rigid polymer films, such as PMMA and PDMS, this new method directly utilizes a graphene film that is more flexible,

while also being free from additional treatments (e.g. heating) used to enhance the contact, which are often required for polymer-transferred graphene.[9]

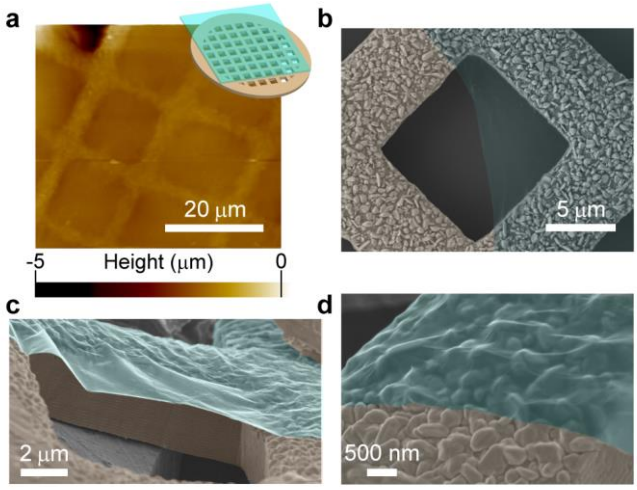

Figure 4 (a) 50 μm × 50 μm AFM image of part of the fabricated graphene TEM grid (schematic in the inset), with a partially-coated window observed in the upper left corner. (b) Top and (c)-(d) side views of false-colored SEM images of a graphene partially-coated window of a TEM grid (graphene in blue). The true color images can be found in SI (section S3, Figure S4).

Graphene Membrane as a Support for TEM Characterization

The two-dimensional ultrathin nature of graphene, and its low atomic number, together with excellent mechanical, thermal and electrical stability, presently make it the ultimate support film for TEM studies.[25, 45-48, 50, 51] Indeed, graphene supports are nearly transparent to electron beams, and enable atomic-resolution imaging of objects, such as biological molecules,[48] gold nanocrystals and its citrate capping agents,[50] or small organic molecules,[51] which would otherwise be very difficult to be observed with TEM using commercial carbon supports.

Herein, we imaged gold nanoparticles (AuNPs) to demonstrate that the suspended graphene membranes obtained with our biphasic method can be used as TEM supports. A

drop of solution containing AuNPs was deposited onto the graphene-coated TEM grid, and left in air to dry before TEM imaging was carried out. Figure 5a shows several AuNPs loaded on the free-standing graphene membrane. They are of regular shape and similar size (~10 nm diameter), as expected. High-resolution TEM characterization was also performed, from which the gold atomic structure and ligands (citrate, blurred surroundings) of a single AuNP can be seen (Figure 5b).

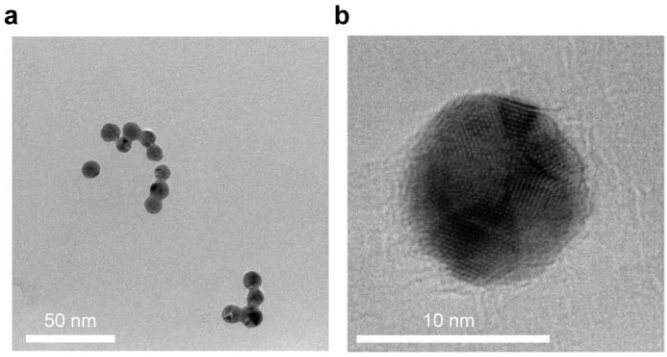

Figure 5 (a) Low-magnification TEM image of gold nanoparticles capped by citrate and (b) high-resolution TEM image of a gold nanoparticle, on a suspended graphene membrane over a Cu TEM grid.

Wetting and Electrochemistry of Supported and Suspended Graphene

The graphene TEM substrate opens up further opportunities of investigating electrochemistry at suspended graphene, for the first time, and comparing the response to that of Cu-supported graphene on the same sample. This is possible using scanning electrochemical cell microscopy (SECCM), which essentially brings a small-scale meniscus electrochemical cell and counter/reference electrodes to a surface (working electrode), allowing electrochemical measurements of unusual electrode materials (see Figure 6a).[52-54]

It is well known that the properties of graphene may be strongly influenced by the supporting substrate; hence studies on free-standing graphene are of enormous interest.[55-57]

The graphene TEM grid was electrochemically tested with two well-known redox couples; (ferrocenylmethyl)trimethylammonium ($FcTMA^{+/2+}$) and hexaammineruthenium ($Ru(NH_3)_6^{3+/2+}$). SECCM utilizes a tapered theta pipet, filled with a solution of interest, such that a meniscus is formed across the two barrels at the end of the pipet. A bias, V_1, is applied between the two quasi-reference counter electrodes (QRCEs, an Ag/AgCl wire inserted into each barrel), to produce an ion conductance/migration current (i_{DC}) between the barrels. When the meniscus comes into contact with the surface of a substrate (working electrode), its potential is controlled by tuning V_2, so that $-(V_1/2+V_2)$ vs. QRCE is the working electrode potential (E) and i_{EC} the corresponding electrochemical current due to any redox reactions. This platform confines the electrochemical cell to sub-micron (nanoscale) dimensions, and allows either the Cu-supported graphene or suspended graphene on the TEM grid to be assessed individually by careful positioning of the SECCM probe in different places of sample.

The SECCM setup was mounted on an inverted microscope, to facilitate the precise navigation and landing of the meniscus onto the graphene film. The pipet was firstly approached near to the graphene sheet, without establishing meniscus contact, by means of a micropositioner. The diffraction of light due to the presence of the pipet was clearly seen through the inverted microscope and used to locate the position of the pipet with respect to the TEM grid (on the suspended graphene or on the supported graphene) (see SI, section S6). From this point, further finer pipet approach was achieved with high control of the *z*-piezo of the SECCM setup. The ion conductance current or i_{DC} can be indicative of the size of the meniscus between pipet and substrate,[41, 52-54] and was used here to diagnose landing of the meniscus on the surface and control of the pipet (as described previously[58]).

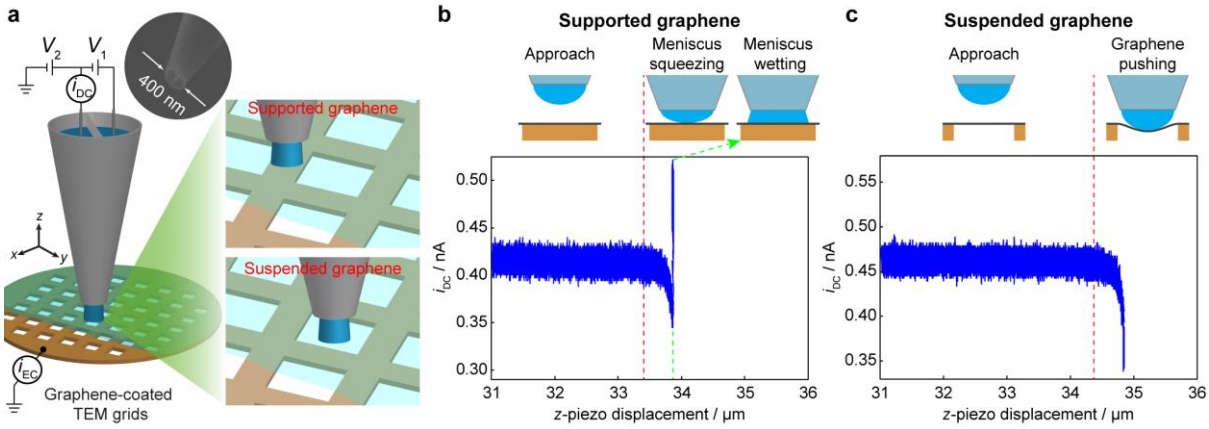

Figure 6 (a) Schematic for an SECCM pipet landing on the supported and suspended parts of a graphene membrane over a Cu TEM grid (not to scale). An SEM image of the end of the type of pipet used is shown as an inset. Typical approach curves demonstrating the change of ion currents (i_{DC}) against *z*-piezo displacement when a pipet meniscus was landed on (b) supported and (c) suspended graphene. The dashed vertical lines indicate the position where the meniscus first contacted the graphene surface (red) and wetted graphene (green, (b)). These approaches are representative of more than 16 measurements carried out for each of these two scenarios.

In Figure 6b and 6c, we show representative approaches of i_{DC} vs. *z*-piezo displacement against supported and suspended graphene (representative of >16 experiments in each case). On the supported graphene (Figure 6b), after the first contact of the meniscus with the conductive substrate (detected through a current spike in the electrochemical current i_{EC}), the meniscus was squeezed against the solid surface, as deduced from the continuous decrease of i_{DC} with the approach.[59] This value dropped by approx. 20 % until a sudden increase in the current was detected at a piezo displacement of ca. 33.9 µm, attributed to the meniscus, under pressure, suddenly wetting the surface. In contrast, when the pipet meniscus came into contact with the suspended graphene sheet (Figure 6c), i_{DC} decreased monotonically by up to

~30 %, during squeezing of the meniscus. This provides some qualitative implications about the difference in the wettability of Cu-supported graphene and suspended graphene.

The wettability of graphene is of considerable interest, given the increasing application of graphene-coated materials. Yet, the relatively few studies available are not in agreement, especially on the effect of the substrate.[29, 60, 61] To the best of our knowledge, the intrinsic wettability of suspended graphene has only been predicted theoretically by molecular dynamics,[62] and has not been measured, due to experimental challenges. Our studies suggest that Cu-supported graphene exhibits stronger wettability compared with a free-standing graphene sheet. This is in line with theoretical studies showing that the contact angle of water on suspended graphene is higher than on Cu-supported graphene.[29, 62-64]

To further investigate the wettability of the suspended graphene membrane, approach and retract experiments were carried out in which the meniscus of an SECCM pipet was pushed further against the graphene with the precise control of the *z*-piezo, while i_{DC} against *z*-piezo displacement was recorded, and the reverse (pull-off) of the meniscus was also measured. An example of these approach and retract curves (with ion conductance current i_{DC} normalized to the initial value of the approach i_{Ini}, i_{DC}/i_{Ini}) is presented in Figure 7 (which is typical of 3 different experiments). The pipet came into contact with the graphene sheet at position 1 on the approach, and as the pushing continued, a gradual decrease of the ionic current is observed due to meniscus compression (as described for Figure 6). The decrease (by ~25 %) stopped at position 2, after which there was a slight increase of the current that we attribute to minor meniscus wetting. This is because the wettability of suspended graphene can be enhanced if strained,[65] and the force on the meniscus between the pipet and graphene may also aid wetting. The pipet was pushed further until position 3, whereupon the translation of the pipet was reversed. Interestingly, there is clearly an attractive interaction between water molecules and the atomically thin carbon sheet as when the pipet was pulled away from the

substrate surface, an increase in i_{DC} is observed (positions 4, 5 and 6), due to the expansion (pulling) of the meniscus formed between SECCM probe and graphene substrate. These observations are consistent with recent theoretical predictions.[61] The meniscus detached at position 7, and the i_{DC} (meniscus confined to the pipet) decreased suddenly to its original value.

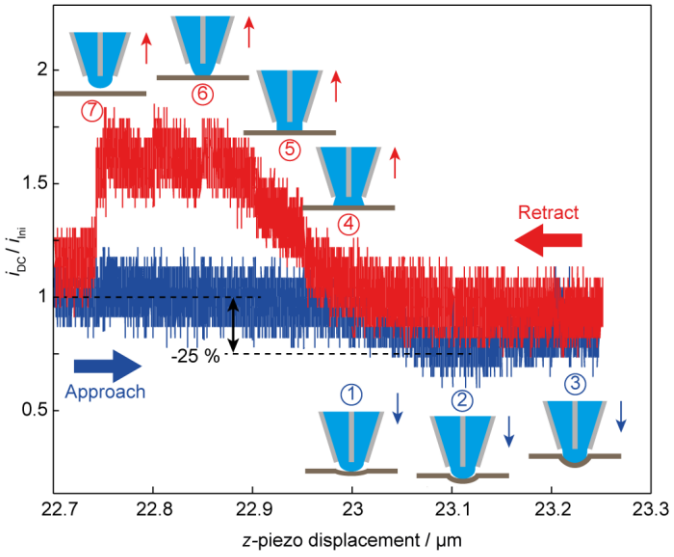

Figure 7 Plot of normalized ion conductance current as a function of the *z*-piezo displacement during the approach and retract processes of an SECCM pipet on suspended graphene.

Suspended graphene devices obtained with our biphasic method, in combination with SECCM, were also employed to study electrochemistry at suspended graphene for the first time. Upon meniscus contact with the graphene sheet, the pipet was held and three cyclic voltammograms (CVs) were recorded at a scan rate of 0.1 V s^{-1} at each landing site for: (i) $FcTMA^{+/2+}$ (oxidation); (ii) $Ru(NH_3)_6^{3+/2+}$ (reduction) in separate experiments (Figure 8). The CVs show the sigmoidal response of a microelectrochemical system with non-linear (spherical segment) diffusion,[41, 53, 66] and are very reproducible. These data are representative

of >6 spot measurements for each of the two couples. For $FcTMA^{+/2+}$, the values of the potential difference between the 3/4 and 1/4-wave potentials ($E_{3/4}$-$E_{1/4}$), which is indicative of the reversibility of the system,[66, 67] was similar on Cu-supported graphene (75 ± 2 mV) and suspended graphene (71 ± 2 mV). With respect to $Ru(NH_3)_6^{3+/2+}$, the CVs on Cu-supported graphene film, led to 69 ± 2 mV for $E_{1/4}$-$E_{3/4}$ and an $E_{1/4}$-$E_{3/4}$ value of 72 ± 2 mV was obtained for suspended graphene. All the CVs observed are characteristic of relatively fast (but not reversible) electron transfer kinetics for $FcTMA^{+/2+}$ and $Ru(NH_3)_6^{3+/2+}$ on the CVD graphene prepared herein, and are broadly in agreement with previous studies on Si/SiO_2- and Cu-supported CVD graphene with the same, and similar, redox species.[22, 68, 69]

Cu-supported graphene and suspended graphene on the TEM grid, along with graphene transferred onto Si/SiO_2 (see SI, section S7), behave in essentially the same way (within experimental error) towards the redox couples studied. There is no detectable substrate effect on the electrochemistry of CVD monolayer graphene, at the spatial resolution of this study. Note that the limiting currents of $FcTMA^{+/2+}$ and $Ru(NH_3)_6^{3+/2+}$ on suspended graphene, are lower than those of Cu-supported graphene. This is due to the different wettability of the supported and suspended graphene membranes, producing different meniscus contact (working electrode) areas and mass transport rates (*vide supra*, Figure 6).

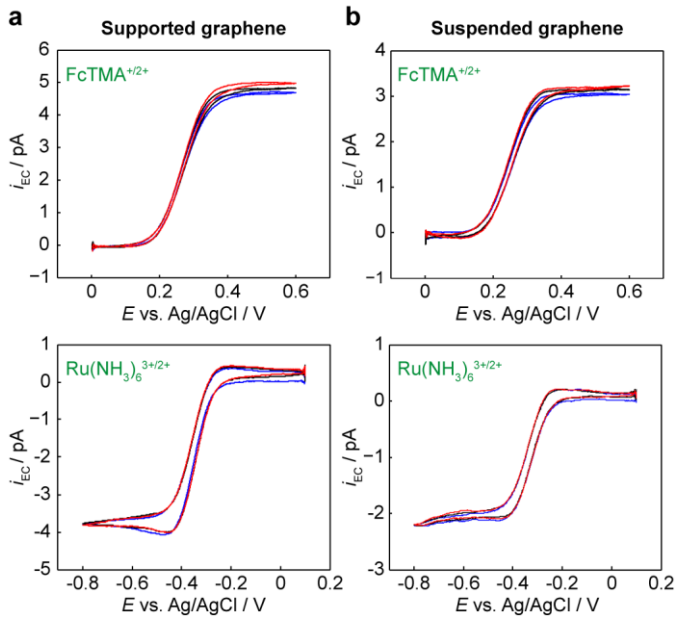

Figure 8 Cyclic voltammograms for the oxidation of 1 mM $FcTMA^+$ and the reduction of 1 mM $Ru(NH_3)_6^{3+}$ in 25 mM KCl, recorded at 0.1 V s^{-1} on (a) supported graphene and (b) suspended graphene. Three consecutive cycles are shown for each case: the 1st (blue), 2nd (black) and 3rd (red) scans. The data are representative of measurements in >6 different locations (spots) for each couple.

Conclusions

A new and efficient polymer-free biphasic (liquid/liquid) method for the transfer of monolayer graphene to a variety of substrates has been demonstrated that opens up new applications and avenues for graphene studies. Key advantages of the method are that the graphene films produced are completely free from any polymer contamination and that detrimental treatments, often associated with polymer-supported transfer routes, are minimized.

The new polymer-free transfer process is easy to implement and we have shown the capability of the method for transferring graphene (of centimetre scale) onto arbitrary substrates, including complex 3D objects, such as AFM tips and TEM grids. The transferred

graphene has been shown to adapt well to the substrate surfaces, resulting in high quality conductive graphene-coated AFM tips and graphene TEM grids. Graphene coating of AFM tips is advantageous compared to metal-coated tips in that the spatial resolution is not compromised, due to the thinness of the graphene layer. Note that although graphene transfer was exemplified with single tips, it should be possible to coat batches (wafers) of AFM probes from the transfer of a single graphene sheet, considering that large area graphene films can be produced by CVD growth. The resulting graphene-coated AFM probes would also be amenable to further covalent functionalization, for example, via the reduction of diazonium molecules, offering a new platform by which to produce probes for molecular recognition applications, as an alternative to the standard thiol modification of gold-coated tips. It is expected that the probes could be further modified into ultramicroelectrodes for use in combined atomic force and scanning electrochemical microscopy (AFM-SECM), among other applications.

Graphene-coated TEM grids have enabled the wettability and electrochemistry of suspended graphene to be explored for the first time, and also provide a powerful platform for high-resolution imaging of nanostructures. The electrochemical activity of suspended graphene (no discernible difference to supported graphene) makes it suitable for use in sensors and other devices. The electrode/TEM grid combination would serve as a powerful platform for the electrodeposition of nanomaterials for subsequent TEM characterization, and it may also be possible to use the transfer method to fabricate cells for in-situ TEM measurements. Further work to explore the graphene coating of soft materials, in particular, could be very worthwhile.

Methods

CVD Growth of Graphene. Monolayer graphene was synthesized in a commercial low-pressure CVD system (NanoCVD 8G, Moorefield Associates, UK). Copper foil (#13382, 25 µm, 99.8%, Alfa Aesar) was cut into ~1 cm × 1 cm square substrates and subsequently cleaned with acetone, propan-2-ol and water before being put into the CVD growth chamber. A purge regime was performed, pumping the system to vacuum and back filling with Ar, five times. Subsequently, the sample was heated to 900 °C as quickly as possible, under a flow of 190 standard cubic centimeters per minute (sccm) Ar and 10 sccm H_2, before maintaining 900 °C for 2 minutes. The temperature was then quickly increased to 1000 °C under the same gas flow conditions. The pressure regime of the system was also changed, and set to maintain a chamber pressure of 10 Torr. The system was left to stabilize for 15 min to anneal the copper foils, before 17 % (of total gas flow) CH_4 was introduced for 10 min, promoting graphene growth. Post-growth, the CH_4 flow was halted, while a flow of 120 sccm Ar and 10 sccm H_2 was still maintained, allowing the system to cool down to 100 °C, at which point the system was vented and the sample was taken into air to cool down to room temperature.

Polymer-free Graphene Transfer. Mechanical polishing was employed to remove the graphene layer that grows on the backside of copper, with sandpaper (Buehler, P 4000), exposing the copper surface and facilitating the subsequent etching. For this purpose, the graphene/Cu sample was gently placed onto the surface of a 0.1 M ammonium persulfate ($(NH_4)_2S_2O_8$, Sigma-Aldrich, ≥98 %) aqueous solution, and a layer of hexane (VWR Chemicals, 99 %) was slowly added on top by means of a syringe. After an appropriate etching time (~12 h) to remove the copper substrate, the graphene layer was left trapped at the interface. The graphene sheet was scooped out with a clean Si/SiO_2 substrate, completing the first transfer step. A second transfer to a new liquid/liquid interface was carried out to

remove any residual salt particles and debris from the back of the graphene layer. This was readily achieved by bringing the graphene-Si/SiO_2 substrate to an interface between hexane and water. The graphene sheet was kept there for 5 h, to aid cleaning. For the coating of AFM tips (RFESP and SNL-10, Bruker) and copper TEM grids (3 mm, 1500 meshes, SPI Supplies), these substrates were temporarily glued onto a small piece of Si/SiO_2 as a support to facilitate manipulation with tweezers and scoop out the graphene sheet. The substrates were left in air briefly to dry before use.

Scanning Electrochemical Cell Microscopy. The main features of the SECCM setup are illustrated in the main text and described elsewhere.[52, 70] A double barrel capillary (1.5 mm o.d., 1.2 mm i.d., TGC150-10, Harvard Apparatus) was pulled to a ~400 nm tapered end, using a CO_2-laser puller (P-2000, Sutter Instruments). The pipet was then silanized in dichlorodimethylsilane ($Si(CH_3)_2Cl_2$, Acros Organics, 99+ %,) to provide a hydrophobic outer wall, before filling with a solution containing the redox species of interest; either 1 mM (ferrocenylmethyl)trimethylammonium hexafluorophosphate ($FcTMAPF_6$) or 1 mM hexaammineruthenium (III) chloride ($Ru(NH_3)_6Cl_3$, Strem Chemicals, 99.00 %) in 25 mM KCl. A data acquisition rate of 390 points per second (each point the average of 256 readings) was achieved using an FPGA card (PCIe-7852R) with a LabVIEW 2013 interface.

Sample Characterization. Raman spectra and map were acquired using a Renishaw inVia micro-Raman microscope fitted with a CCD detector and a 633 nm Ar^+ laser. A laser power of ~6 mW was employed through a 50× magnification lens, resulting in a laser spot size on the graphene surface of ~1 μm in diameter. Field-emission SEM images of SECCM pipets, conductive graphene AFM tips and graphene TEM grids were obtained with a Zeiss Supra 55-VP microscope, at an acceleration voltage of 3 kV, with a secondary electron detector.

AFM imaging of HOPG was carried out with a home-modified Innova AFM (Bruker). The HOPG sample was kindly provided by Prof. R. L. McCreery (University of Alberta, Canada), originating from Dr. A. Moore, Union Carbide (now GE Advanced Ceramics). For TEM imaging, a JEOL JEM-2000FX TEM was used to image the graphene-coated AFM probes. High-resolution TEM images of gold nanoparticles (10 nm diameter, in citrate buffer, Aldrich) on graphene-coated TEM grids were taken using a JEOL JEM-2100 LaB_6 TEM. Both microscopes were operated at 200 kV accelerating voltage.

Conflict of Interest: The authors declare no competing financial interest.

Acknowledgment. We appreciate the Chancellor's International Scholarship from the University of Warwick awarded to GZ. We acknowledge the EPSRC (EP/H023909/1) for funding AGG and RAL, and financial support from Lubrizol to PMK. We also acknowledge support from the European Research Council through ERC-2009-AdG 247143-QUANTIF. We thank Dr. Jonathan Newland for the acquisition of photos and videos, Ashley Page and Minkyung Kang for writing LabVIEW programs and support, and Dr. Yang-Rae Kim for helpful discussions. We also thank Prof. Julie Macpherson, Anatolii Cuharuc and Dr. Jonathan Edgeworth (Moorfield Associates) for advice, general discussions on graphene growth and for providing the CVD reactor. Some of the equipment used in this work was obtained through the Science City Advanced Materials project with support from Advantage West Midlands and the European Regional Development Fund.

Supporting Information Available: Details of the polymer-transfer method, optical and AFM images of CVD monolayer graphene transferred to Si/SiO_2, Raman spectra and map of CVD monolayer graphene, comparison of graphene transferred by the PDMS-assisted route and the new biphasic method, SEM images of graphene-coated TEM grids, light diffraction from a SECCM pipet over a graphene-coated TEM grid, a CV of graphene transferred onto Si/SiO_2,

and a video demonstrating the transfer of graphene. This material is available free of charge via the Internet at http://pubs.acs.org.

Author information

Corresponding Author

* To whom correspondence should be addressed. E-mail: p.r.unwin@warwick.ac.uk; a.g.guell@warwick.ac.uk.

Present Address

AGG.: School of Engineering and Built Environment, Glasgow Caledonian University, Cowcaddens Road, Glasgow, G4 0BA, UK

References and notes

1. Novoselov, K. S.; Geim, A. K.; Morozov, S. V.; Jiang, D.; Zhang, Y.; Dubonos, S. V.; Grigorieva, I. V.; Firsov, A. A. Electric Field Effect in Atomically Thin Carbon Films. *Science* 2004, 306, 666-669.

2. Geim, A. K.; Novoselov, K. S. The Rise of Graphene. *Nat. Mater.* 2007, 6, 183-191.

3. Avouris, P. Graphene: Electronic and Photonic Properties and Devices. *Nano Lett.* 2010, 10, 4285-4294.

4. Lee, C.; Wei, X.; Kysar, J. W.; Hone, J. Measurement of the Elastic Properties and Intrinsic Strength of Monolayer Graphene. *Science* 2008, 321, 385-388.

5. Bunch, J. S.; Verbridge, S. S.; Alden, J. S.; van der Zande, A. M.; Parpia, J. M.; Craighead, H. G.; McEuen, P. L. Impermeable Atomic Membranes from Graphene Sheets. *Nano Lett.* 2008, 8, 2458-2462.

6. Paulus, G. L. C.; Wang, Q. H.; Strano, M. S. Covalent Electron Transfer Chemistry of Graphene with Diazonium Salts. *Acc. Chem. Res.* 2013, 46, 160-170.

7. Elias, D. C.; Nair, R. R.; Mohiuddin, T. M. G.; Morozov, S. V.; Blake, P.; Halsall, M. P.; Ferrari, A. C.; Boukhvalov, D. W.; Katsnelson, M. I.; Geim, A. K.; Novoselov, K. S.

Control of Graphene's Properties by Reversible Hydrogenation: Evidence for Graphane. *Science* 2009, 323, 610-613.

8. Van Noorden, R. Production: Beyond Sticky Tape. *Nature* 2012, 483, S32-S33.

9. Suk, J. W.; Kitt, A.; Magnuson, C. W.; Hao, Y.; Ahmed, S.; An, J.; Swan, A. K.; Goldberg, B. B.; Ruoff, R. S. Transfer of CVD-Grown Monolayer Graphene onto Arbitrary Substrates. *ACS Nano* 2011, 5, 6916-6924.

10. Bae, S.; Kim, H.; Lee, Y.; Xu, X.; Park, J. S.; Zheng, Y.; Balakrishnan, J.; Lei, T.; Kim, H. R.; Song, Y. I.; Kim, Y. J.; Kim, K. S.; Ozyilmaz, B.; Ahn, J. H.; Hong, B. H.; Iijima, S. Roll-to-roll Production of 30-inch Graphene Films for Transparent Electrodes. *Nat. Nanotechnol.* 2010, 5, 574-578.

11. Reina, A.; Jia, X.; Ho, J.; Nezich, D.; Son, H.; Bulovic, V.; Dresselhaus, M. S.; Kong, J. Large Area, Few-Layer Graphene Films on Arbitrary Substrates by Chemical Vapor Deposition. *Nano Lett.* 2009, 9, 30-35.

12. Sutter, P. W.; Flege, J.-I.; Sutter, E. A. Epitaxial Graphene on Ruthenium. *Nat. Mater.* 2008, 7, 406-411.

13. Li, X.; Cai, W.; An, J.; Kim, S.; Nah, J.; Yang, D.; Piner, R.; Velamakanni, A.; Jung, I.; Tutuc, E.; Banerjee, S. K.; Colombo, L.; Ruoff, R. S. Large-Area Synthesis of High-Quality and Uniform Graphene Films on Copper Foils. *Science* 2009, 324, 1312-1314.

14. Zhang, Y.; Zhang, L.; Zhou, C. Review of Chemical Vapor Deposition of Graphene and Related Applications. *Acc. Chem. Res.* 2013, 46, 2329-2339.

15. Kang, J.; Shin, D.; Bae, S.; Hong, B. H. Graphene Transfer: Key for Applications. *Nanoscale* 2012, 4, 5527-5537.

16. Wang, Y.; Zheng, Y.; Xu, X.; Dubuisson, E.; Bao, Q.; Lu, J.; Loh, K. P. Electrochemical Delamination of CVD-Grown Graphene Film: Toward the Recyclable Use of Copper Catalyst. *ACS Nano* 2011, 5, 9927-9933.

17. Cherian, C. T.; Giustiniano, F.; Martin-Fernandez, I.; Andersen, H.; Balakrishnan, J.; Özyilmaz, B. 'Bubble-Free' Electrochemical Delamination of CVD Graphene Films. *Small* 2015, 11, 189-194.

18. Li, X.; Zhu, Y.; Cai, W.; Borysiak, M.; Han, B.; Chen, D.; Piner, R. D.; Colombo, L.; Ruoff, R. S. Transfer of Large-Area Graphene Films for High-Performance Transparent Conductive Electrodes. *Nano Lett.* 2009, 9, 4359-4363.

19. Kim, K. S.; Zhao, Y.; Jang, H.; Lee, S. Y.; Kim, J. M.; Kim, K. S.; Ahn, J.-H.; Kim, P.; Choi, J.-Y.; Hong, B. H. Large-scale Pattern Growth of Graphene Films for Stretchable Transparent Electrodes. *Nature* 2009, 457, 706-710.

20. Park, H. J.; Meyer, J.; Roth, S.; Skákalová, V. Growth and Properties of Few-layer Graphene Prepared by Chemical Vapor Deposition. *Carbon* 2010, 48, 1088-1094.

21. Lin, Y.-C.; Lu, C.-C.; Yeh, C.-H.; Jin, C.; Suenaga, K.; Chiu, P.-W. Graphene Annealing: How Clean Can It Be? *Nano Lett.* 2012, 12, 414-419.

22. Li, W.; Tan, C.; Lowe, M. A.; Abruña, H. D.; Ralph, D. C. Electrochemistry of Individual Monolayer Graphene Sheets. *ACS Nano* 2011, 5, 2264-2270.

23. Pirkle, A.; Chan, J.; Venugopal, A.; Hinojos, D.; Magnuson, C. W.; McDonnell, S.; Colombo, L.; Vogel, E. M.; Ruoff, R. S.; Wallace, R. M. The Effect of Chemical Residues on the Physical and Electrical Properties of Chemical Vapor Deposited Graphene Transferred to SiO_2. *Appl. Phys. Lett.* 2011, 99, 122108.

24. Suk, J. W.; Lee, W. H.; Lee, J.; Chou, H.; Piner, R. D.; Hao, Y.; Akinwande, D.; Ruoff, R. S. Enhancement of the Electrical Properties of Graphene Grown by Chemical Vapor Deposition via Controlling the Effects of Polymer Residue. *Nano Lett.* 2013, 13, 1462-1467.

25. Regan, W.; Alem, N.; Alemán, B.; Geng, B.; Girit, Ç.; Maserati, L.; Wang, F.; Crommie, M.; Zettl, A. A Direct Transfer of Layer-area Graphene. *Appl. Phys. Lett.* 2010, 96, 113102.

26. Lin, W.-H.; Chen, T.-H.; Chang, J.-K.; Taur, J.-I.; Lo, Y.-Y.; Lee, W.-L.; Chang, C.-S.; Su, W.-B.; Wu, C.-I. A Direct and Polymer-Free Method for Transferring Graphene Grown by Chemical Vapor Deposition to Any Substrate. *ACS Nano* 2014, 8, 1784-1791.

27. Toth, P. S.; Ramasse, Q. M.; Velicky, M.; Dryfe, R. A. W. Functionalization of Graphene at the Organic/Water Interface. *Chem. Sci.* 2015, 6, 1316-1323.

28. Wang, Q. H.; Jin, Z.; Kim, K. K.; Hilmer, A. J.; Paulus, G. L. C.; Shih, C.-J.; Ham, M.-H.; Sanchez-Yamagishi, J. D.; Watanabe, K.; Taniguchi, T.; Kong, J.; Jarillo-Herrero, P.; Strano, M. S. Understanding and Controlling the Substrate Effect on Graphene Electron-transfer Chemistry via Reactivity Imprint Lithography. *Nat. Chem.* 2012, 4, 724-732.

29. Rafiee, J.; Mi, X.; Gullapalli, H.; Thomas, A. V.; Yavari, F.; Shi, Y.; Ajayan, P. M.; Koratkar, N. A. Wetting Transparency of Graphene. *Nat. Mater*. 2012, 11, 217-222.

30. Lupina, G.; Kitzmann, J.; Costina, I.; Lukosius, M.; Wenger, C.; Wolff, A.; Vaziri, S.; Ostling, M.; Pasternak, I.; Krajewska, A.; Strupinski, W.; Kataria, S.; Gahoi, A.; Lemme, M. C.; Ruhl, G.; Zoth, G.; Luxenhofer, O.; Mehr, W. Residual Metallic Contamination of Transferred Chemical Vapor Deposited Graphene. *ACS Nano* 2015, 9, 4776-4785.

31. Lange, N. A.; Forker, G. M. *Lange's Handbook of Chemistry*. 10th ed.; 1967.

32. Gao, L.; Ni, G.-X.; Liu, Y.; Liu, B.; Castro Neto, A. H.; Loh, K. P. Face-to-face Transfer of Wafer-scale Graphene Films. *Nature* 2014, 505, 190-194.

33. Ferrari, A. C.; Basko, D. M. Raman Spectroscopy as a Versatile Tool for Studying the Properties of Graphene. *Nat. Nanotechnol.* 2013, 8, 235-246.

34. Xu, K.; Cao, P.; Heath, J. R. Graphene Visualizes the First Water Adlayers on Mica at Ambient Conditions. *Science* 2010, 329, 1188-1191.

35. Zong, Z.; Chen, C.-L.; Dokmeci, M. R.; Wan, K.-t. Direct Measurement of Graphene Adhesion on Silicon Surface by Intercalation of Nanoparticles. *J. Appl. Phys.* 2010, 107, 026104.

36. Mohanty, N.; Fahrenholtz, M.; Nagaraja, A.; Boyle, D.; Berry, V. Impermeable Graphenic Encasement of Bacteria. *Nano Lett.* 2011, 11, 1270-1275.

37. Khatib, O.; Wood, J. D.; McLeod, A. S.; Goldflam, M. D.; Wagner, M.; Damhorst, G. L.; Koepke, J. C.; Doidge, G. P.; Rangarajan, A.; Bashir, R.; Pop, E.; Lyding, J. W.; Thiemens, M. H.; Keilmann, F.; Basov, D. N. Graphene-Based Platform for Infrared Near-Field Nanospectroscopy of Water and Biological Materials in an Aqueous Environment. *ACS Nano* 2015, 9, 7968-7975.

38. Wold, D. J.; Frisbie, C. D. Fabrication and Characterization of Metal−Molecule−Metal Junctions by Conducting Probe Atomic Force Microscopy. *J. Am. Chem. Soc.* 2001, 123, 5549-5556.

39. Xu, D.; Watt, G. D.; Harb, J. N.; Davis, R. C. Electrical Conductivity of Ferritin Proteins by Conductive AFM. *Nano Lett.* 2005, 5, 571-577.

40. Patel, A. N.; Collignon, M. G.; O'Connell, M. A.; Hung, W. O.; McKelvey, K.; Macpherson, J. V.; Unwin, P. R. A New View of Electrochemistry at Highly Oriented Pyrolytic Graphite. *J. Am. Chem. Soc.* 2012, 134, 20117-20130.

41. Güell, A. G.; Cuharuc, A. S.; Kim, Y.-R.; Zhang, G.; Tan, S.-y.; Ebejer, N.; Unwin, P. R. Redox-Dependent Spatially Resolved Electrochemistry at Graphene and Graphite Step Edges. *ACS Nano* 2015, 9, 3558-3571.

42. Banerjee, S.; Sardar, M.; Gayathri, N.; Tyagi, A. K.; Raj, B. Conductivity Landscape of Highly Oriented Pyrolytic Graphite Surfaces Containing Ribbons and Edges. *Phys. Rev. B* 2005, 72, 075418.

43. Lu, Y.; Muñoz, M.; Steplecaru, C. S.; Hao, C.; Bai, M.; Garcia, N.; Schindler, K.; Esquinazi, P. Electrostatic Force Microscopy on Oriented Graphite Surfaces: Coexistence of Insulating and Conducting Behaviors. *Phys. Rev. Lett.* 2006, 97, 076805.

44. Wen, Y.; Chen, J.; Guo, Y.; Wu, B.; Yu, G.; Liu, Y. Multilayer Graphene-coated Atomic Force Microscopy Tips for Molecular Junctions. *Adv. Mater.* 2012, 24, 3482-3485.

45. Wilson, N. R.; Pandey, P. A.; Beanland, R.; Young, R. J.; Kinloch, I. A.; Gong, L.; Liu, Z.; Suenaga, K.; Rourke, J. P.; York, S. J.; Sloan, J. Graphene Oxide: Structural Analysis and Application as a Highly Transparent Support for Electron Microscopy. *ACS Nano* 2009, 3, 2547-2556.

46. van de Put, M. W. P.; Patterson, J. P.; Bomans, P. H. H.; Wilson, N. R.; Friedrich, H.; van Benthem, R. A. T. M.; de With, G.; O'Reilly, R. K.; Sommerdijk, N. A. J. M. Graphene Oxide Single Sheets as Substrates for High Resolution CryoTEM. *Soft Matter* 2015, 11, 1265-1270.

47. Buckhout-White, S.; Robinson, J. T.; Bassim, N. D.; Goldman, E. R.; Medintz, I. L.; Ancona, M. G. TEM Imaging of Unstained DNA Nanostructures Using Suspended Graphene. *Soft Matter* 2013, 9, 1414-1417.

48. Nair, R. R.; Blake, P.; Blake, J. R.; Zan, R.; Anissimova, S.; Bangert, U.; Golovanov, A. P.; Morozov, S. V.; Geim, A. K.; Novoselov, K. S.; Latychevskaia, T. Graphene as a Transparent Conductive Support for Studying Biological Molecules by Transmission Electron Microscopy. *Appl. Phys. Lett.* 2010, 97, 153102.

49. Meyer, J. C.; Girit, C. O.; Crommie, M. F.; Zettl, A. Hydrocarbon Lithography on Graphene Membranes. *Appl. Phys. Lett.* 2008, 92, 123110.

50. Lee, Z.; Jeon, K.-J.; Dato, A.; Erni, R.; Richardson, T. J.; Frenklach, M.; Radmilovic, V. Direct Imaging of Soft-Hard Interfaces Enabled by Graphene. *Nano Lett.* 2009, 9, 3365-3369.

51. Meyer, J. C.; Girit, C. O.; Crommie, M. F.; Zettl, A. Imaging and Dynamics of Light Atoms and Molecules on Graphene. *Nature* 2008, 454, 319-322.

52. Ebejer, N.; Güell, A. G.; Lai, S. C.; McKelvey, K.; Snowden, M. E.; Unwin, P. R. Scanning Electrochemical Cell Microscopy: A Versatile Technique for Nanoscale Electrochemistry and Functional Imaging. *Annu. Rev. Anal. Chem.* 2013, 6, 329-351.

53. Snowden, M. E.; Güell, A. G.; Lai, S. C.; McKelvey, K.; Ebejer, N.; O'Connell, M. A.; Colburn, A. W.; Unwin, P. R. Scanning Electrochemical Cell Microscopy: Theory and Experiment for Quantitative High Resolution Spatially-resolved Voltammetry and Simultaneous Ion-conductance Measurements. *Anal. Chem.* 2012, 84, 2483-2491.

54. Lai, S. C. S.; Patel, A. N.; McKelvey, K.; Unwin, P. R. Definitive Evidence for Fast Electron Transfer at Pristine Basal Plane Graphite from High-Resolution Electrochemical Imaging. *Angew. Chem. Int. Ed.* 2012, 51, 5405-5408.

55. Cai, W.; Moore, A. L.; Zhu, Y.; Li, X.; Chen, S.; Shi, L.; Ruoff, R. S. Thermal Transport in Suspended and Supported Monolayer Graphene Grown by Chemical Vapor Deposition. *Nano Lett.* 2010, 10, 1645-1651.

56. Ni, Z. H.; Yu, T.; Luo, Z. Q.; Wang, Y. Y.; Liu, L.; Wong, C. P.; Miao, J.; Huang, W.; Shen, Z. X. Probing Charged Impurities in Suspended Graphene Using Raman Spectroscopy. *ACS Nano* 2009, 3, 569-574.

57. Guimaraes, M. H.; Veligura, A.; Zomer, P. J.; Maassen, T.; Vera-Marun, I. J.; Tombros, N.; van Wees, B. J. Spin Transport in High-quality Suspended Graphene Devices. *Nano Lett.* 2012, 12, 3512-3517.

58. Zhang, G.; Kirkman, P. M.; Patel, A. N.; Cuharuc, A. S.; McKelvey, K.; Unwin, P. R. Molecular Functionalization of Graphite Surfaces: Basal Plane versus Step Edge Electrochemical Activity. *J. Am. Chem. Soc.* 2014, 136, 11444-11451.

59. Chen, C.-H.; Meadows, K. E.; Cuharuc, A.; Lai, S. C. S.; Unwin, P. R. High Resolution Mapping of Oxygen Reduction Reaction Kinetics at Polycrystalline Platinum Electrodes. *Phys. Chem. Chem. Phys.* 2014, 16, 18545-18552.

60. Raj, R.; Maroo, S. C.; Wang, E. N. Wettability of Graphene. *Nano Lett.* 2013, 13, 1509-1515.

61. Hung, S.-W.; Hsiao, P.-Y.; Chen, C.-P.; Chieng, C.-C. Wettability of Graphene-Coated Surface: Free Energy Investigations Using Molecular Dynamics Simulation. *J. Phys. Chem. C* 2015, 119, 8103-8111.

62. Shih, C.-J.; Wang, Q. H.; Lin, S.; Park, K.-C.; Jin, Z.; Strano, M. S.; Blankschtein, D. Breakdown in the Wetting Transparency of Graphene. *Phys. Rev. Lett.* 2012, 109, 176101.

63. Mugele, F. Wetting: Unobtrusive Graphene Coatings. *Nat. Mater.* 2012, 11, 182-183.

64. Li, Z.; Wang, Y.; Kozbial, A.; Shenoy, G.; Zhou, F.; McGinley, R.; Ireland, P.; Morganstein, B.; Kunkel, A.; Surwade, S. P.; Li, L.; Liu, H. Effect of Airborne Contaminants on the Wettability of Supported Graphene and Graphite. *Nat. Mater.* 2013, 12, 925-931.

65. Ma, M.; Tocci, G.; Michaelides, A.; Aeppli, G. Fast Diffusion of Water Nanodroplets on Graphene. *Nat. Mater*. 2016, 15, 66-71.

66. A. J. Bard; Faulkner, L. R. *Electrochemical Methods: Fundamentals and Applications*. 2nd ed.; John Wiley& Sons, Inc.: New York, 2001.

67. Güell, A. G.; Ebejer, N.; Snowden, M. E.; Macpherson, J. V.; Unwin, P. R. Structural Correlations in Heterogeneous Electron Transfer at Monolayer and Multilayer Graphene Electrodes. *J. Am. Chem. Soc.* 2012, 134, 7258-7261.

68. Zhong, J.-H.; Zhang, J.; Jin, X.; Liu, J.-Y.; Li, Q.; Li, M.-H.; Cai, W.; Wu, D.-Y.; Zhan, D.; Ren, B. Quantitative Correlation between Defect Density and Heterogeneous Electron Transfer Rate of Single Layer Graphene. *J. Am. Chem. Soc.* 2014, 136, 16609-16617.

69. Bosch-Navarro, C.; Laker, Z. P. L.; Rourke, J. P.; Wilson, N. R. Reproducible, Stable and Fast Electrochemical Activity from Easy to Make Graphene on Copper Electrodes. *Phys. Chem. Chem. Phys.* 2015, 17, 29628-29636.

70. Ebejer, N.; Schnippering, M.; Colburn, A. W.; Edwards, M. A.; Unwin, P. R. Localized High Resolution Electrochemistry and Multifunctional Imaging: Scanning Electrochemical Cell Microscopy. *Anal. Chem.* 2010, 82, 9141-9145.

Graphical Table of Contents

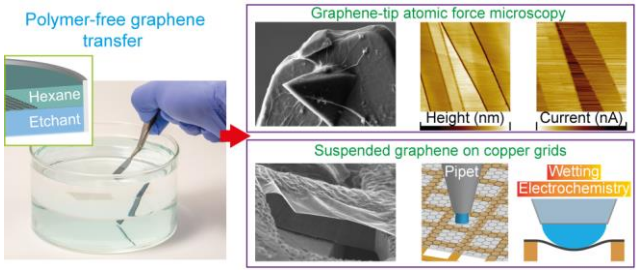

Supporting Information

Versatile Polymer-Free Graphene Transfer Method and Applications

Guohui Zhang, † Aleix G. Güell, † * Paul M. Kirkman, Robert A. Lazenby, Thomas S. Miller and Patrick R. Unwin*

Department of Chemistry, University of Warwick, Coventry, CV4 7AL, United Kingdom.

* To whom correspondence should be addressed. Email: p.r.unwin@warwick.ac.uk; a.g.guell@warwick.ac.uk.

† These authors contributed equally.

Contents

S1 | Operation of the Polymer-free Method Page S-2

S2 | Optical and AFM Characterization of CVD Graphene on Si/SiO_2 Page S-3

S3 | Raman Characterization of CVD Monolayer Graphene Page S-4

S4 | PDMS-assisted Graphene Transfer Page S-5

S5 | Graphene-coated TEM Grids Page S-7

S6 | Optical Views of an SECCM Pipet Approaching Towards Cu-supported Graphene and Suspended Graphene Page S-9

S7 | Electrochemistry of Si/SiO_2-supported Graphene Page S-10

References Page S-11

S1 | Operation of the Polymer-free Method

To transfer the freestanding graphene layer, the substrate of choice was positioned across the interface in an angle (~45^{o}), to the edge of the graphene film, and was withdrawn from the solution in a single slow motion, while maintaining a low force on the graphene sample, as shown in Figure S1. This ensured that a complete graphene film was transferred.

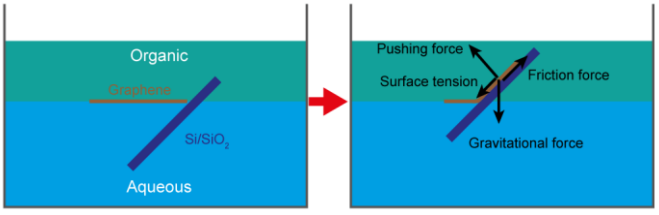

Figure S1 Schematic of the scooping of graphene from the polymer-free transfer method.

S2 | Optical and AFM Characterization of CVD Graphene on Si/SiO_2

As evident by the optical image (Figure S2a), a complete graphene film can be transferred onto Si/SiO_2 using our polymer-free method, with tears and wrinkles only occasionally seen. AFM imaging revealed a good cleanliness of graphene surface after transfer (Figure S2b), with no obvious residues observed, usually associated with polymer-supported methods.

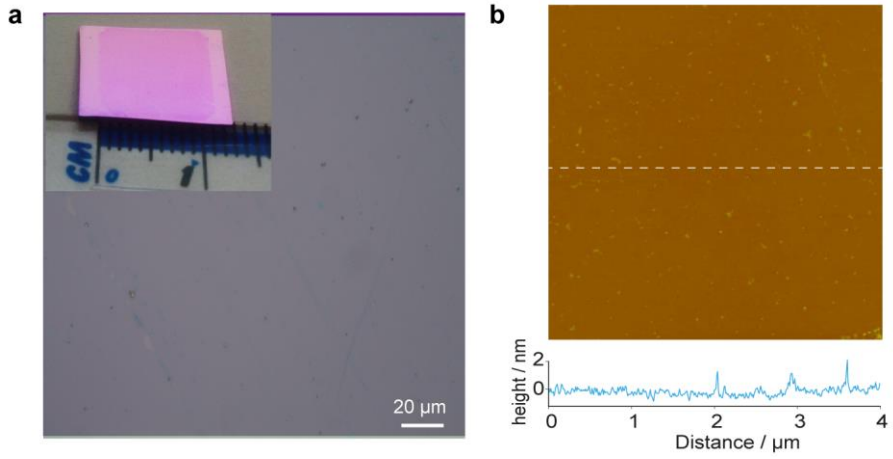

Figure S2 (a) Optical microscope and (b) AFM images of transferred graphene on Si/SiO_2 using the polymer-free transfer method.

S3 | Raman Characterization of CVD Monolayer Graphene

Raman spectroscopy measurements were carried out on as-grown graphene/Cu samples and graphene transferred onto Si/SiO_2 using the biphasic method (Figure S3). These spectra highlight the high-quality CVD growth and efficient transfer of monolayer graphene (see main text).[1]

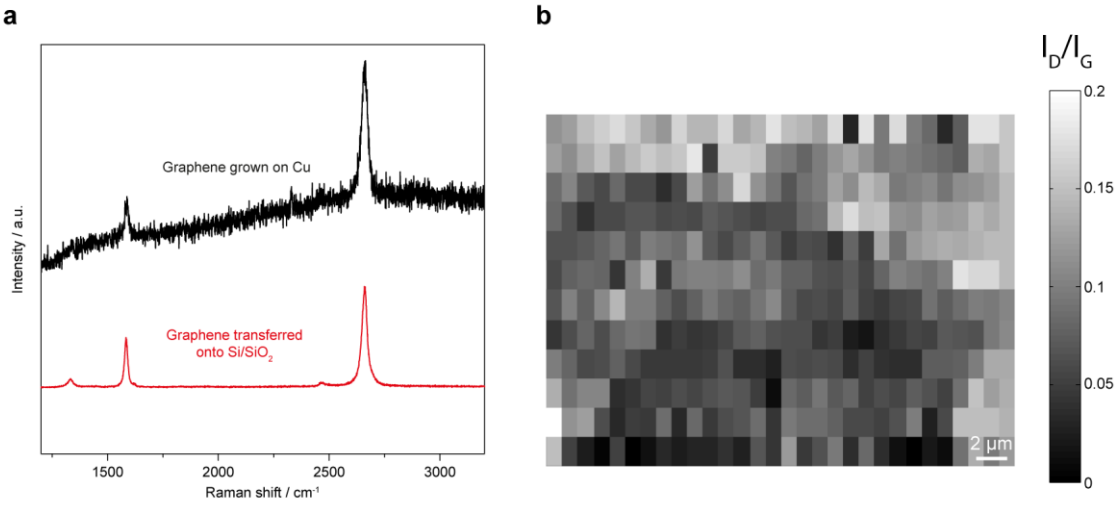

Figure S3 (a) Raman spectra of as-grown graphene film on copper, and fully transferred graphene on Si/SiO_2 by the new polymer-free biphasic method. (b) Raman mapping of graphene on Si/SiO_2.

S4 | PDMS-assisted Graphene Transfer

The PDMS-assisted transfer method has been reported to be a most developed methodology in the literature,[2, 3] and is widely adopted in the graphene community. It was important to demonstrate that the polymer-free biphasic transfer method did not produce more mechanically-introduced defects in the graphene, as compared to this polymer-support route. Thus, comparative experiments using a traditional PDMS-supported transfer process were carried out. Graphene samples were synthesized under the same CVD chamber conditions as used for biphasic transfer studies, to ensure the starting material was of the same quality. The as-grown graphene/Cu samples were polished on the back, as described in main text, and then coated with a PDMS layer. For the preparation of PDMS films, the pre-polymer and curing agent (Sylgard 184 elastomer), with a ratio of 10:1 (w/w), were fully mixed in a petri dish and then degassed in a desiccator for 30 min. A tiny amount of the mixture was poured slowly onto the front side of the sample, developing a thin layer on top of the graphene, and the sample was then kept at 70 °C in an oven for one hour. After cooling down, the PDMS-coated sample was gently laid on the surface of 0.1 M $(NH_4)_2S_2O_8$ aqueous solution, with the polymer side facing up, and wet etched for the same period of time (~12 h) as our biphasic method. The sample was subsequently transferred to pure water with the aid of an Si/SiO_2 wafer, to remove possible salt contaminants. After an appropriate time (~5 h), the sample was scooped out using an Si/SiO_2 wafer and left in air to dry. Representative Raman spectra for the graphene films, produced by both the PDMS-supported route and the biphasic method (main text), are presented in Figure S4. There is no noticeable difference in the intrinsic quality of the graphene films, as indicated by the I_D/I_G ratios of < 0.2. Full width at half-maximum values of 36 cm^{-1} (PDMS route) and 28 cm^{-1} (biphasic route) for the 2D band were indicative of monolayer graphene.[4] Significantly, considering the PDMS block had not been dissolved with organic solvents for the PDMS/graphene sample, a process which could

introduce further defects, it is clear that the biphasic approach is capable of producing transferred graphene films on Si/SiO_2 of at least similar quality to those transferred using traditional polymer-supported routes, while eliminating the polymer residue problem.

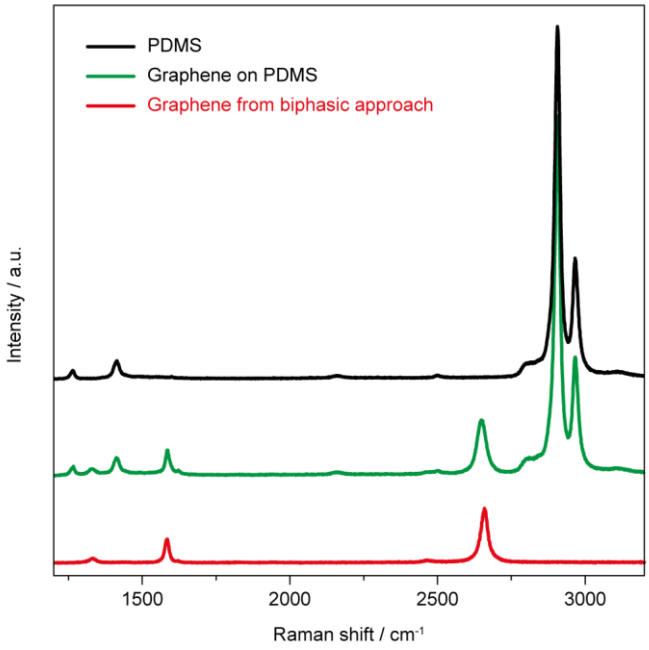

Figure S4 Raman spectra of PDMS, graphene on PDMS and graphene transferred onto Si/SiO_2 using the polymer-free biphasic approach.

S5 | Graphene-coated TEM Grids

Graphene-coated TEM grids were characterized with SEM. Windows with a full coverage of graphene were observed, indicating the production of extensive areas of continuous suspended graphene membranes (Figure S5).

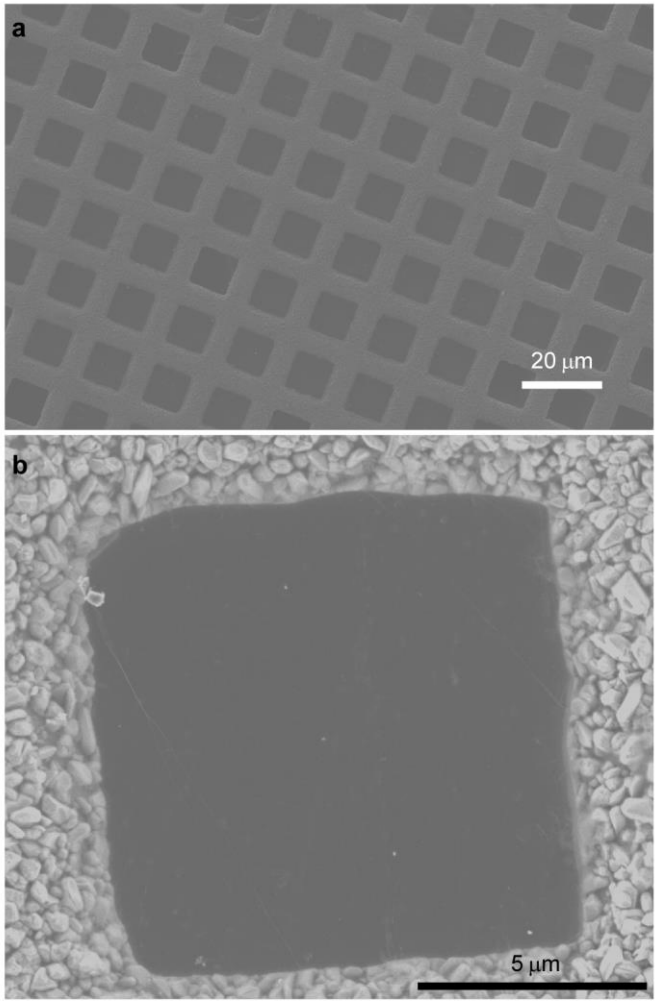

Figure S5 SEM image of (a) part of a graphene-coated TEM grid and (b) a graphene fully-covered window on the grid.

The true color SEM images for Figure 4b-4d in main text are shown in Figure S6, demonstrating the transparent suspended graphene membrane over the holes and the highly adaptable coating of a graphene sheet on the metal structure of a TEM grid, obtained with the biphasic transfer method.

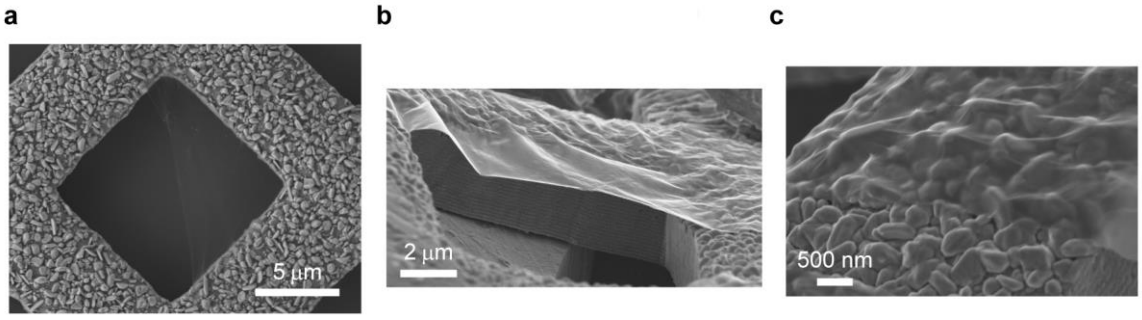

Figure S6 (a) Top and (b)-(c) side views of SEM images of a graphene partially-coated window of a TEM grid.

S6 | Optical Views of an SECCM Pipet Approaching Towards Cu-supported Graphene and Suspended Graphene

An inverted optical microscope was used to aid the positioning of the SECCM pipet over a graphene-coated TEM grid. Different light diffraction patterns from the end of the pipet were observed when the pipet was approaching Cu-supported graphene (Figure S7a) and suspended graphene (Figure S7b).

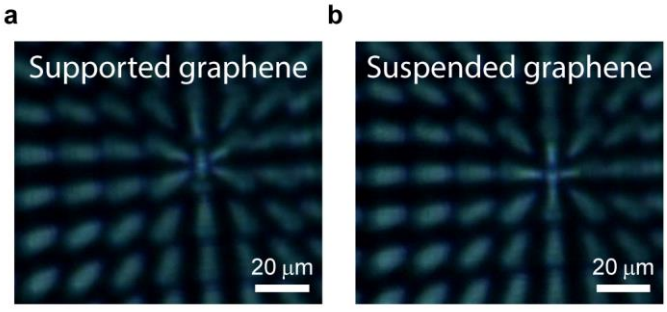

Figure S7 Inverted optical microscope view of the light diffraction from the end of the pipet positioned near (a) Cu-supported graphene and (b) suspended graphene.

S7 | Electrochemistry of Si/SiO_2-supported Graphene

Cyclic voltammetry (CV) measurements using an SECCM setup (~400 nm pipet) were also carried out on the graphene transferred onto Si/SiO_2, which is usually the support for electrochemistry studies of graphene.[5-7] A typical CV for the oxidation of 1 mM $FcTMA^+$ is shown in Figure S8, with a potential difference between the 3/4 and 1/4–wave potentials ($E_{3/4}$-$E_{1/4}$) of 70 ± 2 mV obtained. This value is reasonably close to the reversible limit and similar to that obtained for Cu-supported graphene and suspended graphene in this work (see main text) and other studies.[5]

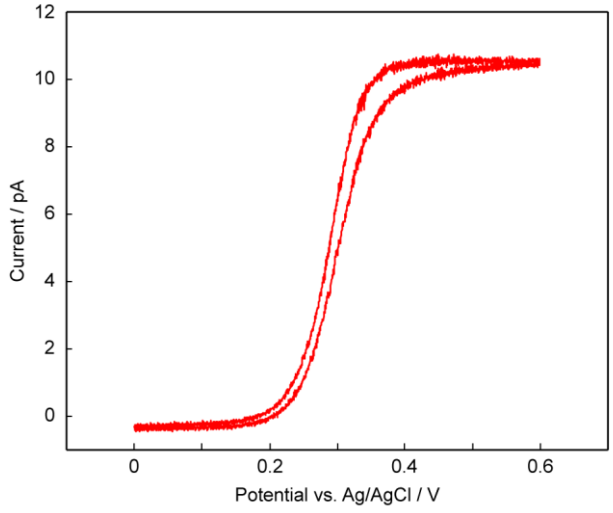

Figure S8 An SECCM cyclic voltammogram for the oxidation of 1 mM $FcTMA^+$ in 25 mM KCl on the graphene transferred onto Si/SiO_2, recorded at a scan rate of 0.1 V s^{-1}.

References

1. Kim, K. S.; Zhao, Y.; Jang, H.; Lee, S. Y.; Kim, J. M.; Kim, K. S.; Ahn, J.-H.; Kim, P.; Choi, J.-Y.; Hong, B. H. Large-scale Pattern Growth of Graphene Films for Stretchable Transparent Electrodes. *Nature* 2009, 457, 706-710.

2. Oznuluer, T.; Pince, E.; Polat, E. O.; Balci, O.; Salihoglu, O.; Kocabas, C. Synthesis of Graphene on Gold. *Appl. Phys. Lett.* 2011, 98, 183101.

3. Ching-Yuan, S.; Dongliang, F.; Ang-Yu, L.; Keng-Ku, L.; Yanping, X.; Zhen-Yu, J.; Lain-Jong, L. Transfer Printing of Graphene Strip from the Graphene Grown on Copper Wires. *Nanotechnology* 2011, 22, 185309.

4. Güell, A. G.; Ebejer, N.; Snowden, M. E.; Macpherson, J. V.; Unwin, P. R. Structural Correlations in Heterogeneous Electron Transfer at Monolayer and Multilayer Graphene Electrodes. *J. Am. Chem. Soc.* 2012, 134, 7258-7261.

5. Li, W.; Tan, C.; Lowe, M. A.; Abruña, H. D.; Ralph, D. C. Electrochemistry of Individual Monolayer Graphene Sheets. *ACS Nano* 2011, 5, 2264-2270.

6. Valota, A. T.; Kinloch, I. A.; Novoselov, K. S.; Casiraghi, C.; Eckmann, A.; Hill, E. W.; Dryfe, R. A. W. Electrochemical Behavior of Monolayer and Bilayer Graphene. *ACS Nano* 2011, 5, 8809-8815.

7. Güell, A. G.; Cuharuc, A. S.; Kim, Y.-R.; Zhang, G.; Tan, S.-y.; Ebejer, N.; Unwin, P. R. Redox-Dependent Spatially Resolved Electrochemistry at Graphene and Graphite Step Edges. *ACS Nano* 2015, 9, 3558-3571.